Available online at www.sciencedirect.com
ScienceDirect
Mathematics and Computers in Simulation 194 (2022) 124–140
MATHEMATICS AND COMPUTERS IN SIMULATION
www.elsevier.com/locate/matcom

Original articles

Local thermal non-equilibrium (LTNE) effects on thermal-free convection in a nanofluid-saturated horizontal elliptical non-Darcian porous annulus

Tahar Tayebi[a,b], Ali J. Chamkha[c,d], Hakan F. Öztop[e,f,*], Lynda Bouzeroura[g]

[a] *Faculty of Sciences and Technology, University of Bordj Bou Arreridj, 34030, Algeria*
[b] *Energy Physics Laboratory, Department of Physics, Exact Sciences Faculty, University of Frères Mentouri Constantine1, 25000 Constantine, Algeria*
[c] *Faculty of Engineering, Kuwait College of Science and Technology, Doha District, Kuwait*
[d] *Center of Excellence in Desalination Technology, King Abdulaziz University, P.O. Box 80200, Jeddah 21589, Saudi Arabia*
[e] *Department of Mechanical Engineering, Technology Faculty, Fırat University, Elazig, Turkey*
[f] *Department of Medical Research, China Medical University Hospital, China Medical University, Taichung, Taiwan*
[g] *LEZINRU, Faculty of ECMS, University of Bordj Bou Arreridj, 34030, Algeria*

Received 12 September 2021; received in revised form 4 November 2021; accepted 9 November 2021
Available online 16 November 2021

Abstract

In this investigation, a comprehensive and accurate numerical analysis of the local thermal non-equilibrium effects on the natural convection characteristics in a horizontal elliptical porous annulus saturated with nanofluid has been carried out using finite volume technique. The internal surface is isothermally heated while the external one is fixed at uniform lower temperature. The nanofluid phase and the solid phase of the porous structure are out of local thermal equilibrium situation. The heat and the hydrodynamics equations in their dimensionless form under Darcy–Brinkman Forchheimer model were solved computationally by the finite volume technique using the standard SIMPLER algorithm. The results have been examined for various porous medium properties under the LTNE condition. The standard 0.05 significance level was used to identify the local thermal equilibrium within the system. According to the obtained results, the higher the Darcy number and the smaller the non-dimensional heat transfer coefficient for the solid/nanofluid interface, the modified thermal conductivity ratio and the media's porosity, the higher are the LTNE effects. In addition, the spatial distribution contours of the LTNE sources within the porous annulus were schematized.

Keywords: Natural convection; Nanofluid; Thermal local non-equilibrium (LTNE); Darcy–Forchheimer model; Elliptical annulus

1. Introduction

Because of the numerous industrial applications including thermal isolation, heat exchangers, electronic components cooling, thermal reservoirs, petroleum processing, groundwater, drying, nuclear reactors, solar energy,

* Corresponding author at: Department of Mechanical Engineering, Technology Faculty, Fırat University, Elazig, Turkey.
E-mail address: hfoztop1@gmail.com (H.F. Öztop).

https://doi.org/10.1016/j.matcom.2021.11.011

fuel cells, building energy technology, combustion technology, and so on [17,25,28,33,34,37], the process of convective transport in porous materials is a very active field of research. The importance of the convective transport in porous materials has attracted numerical, analytical, and experimental studies in recent years in order to improve the efficiency of their utilization in industrial applications [4,18,21,22,29,31,32,35,41–43,46].

It is said that thermal-convection in porous materials saturated by fluids occurs in local thermal equilibrium (LTE) when the temperatures of the rigid matrix and those of the fluid phase in the porous structure are identical and similar throughout the study domain. Otherwise, heat transfer in the porous media is carried out outside of the local thermal equilibrium (LTNE). From a practical standpoint, the LTNE approach is important in porous media applications such as cooling computer microprocessors with porous metal foams [10], food drying/freezing [47], microwave heating [13], and so on.

Many computational, theoretical, and experimental studies have been conducted to better understand the thermo-convection mechanism within fully or partially porous systems saturated with different fluids under the LTNE approach. In this inventory, we expose some most recent works related to our study. Badruddin et al. [9] employed FEM to computationally examine the heat transport caused by LTE and LTNE in a porous annulus with a square section. The LTNE effects are determined by using an extra heat equation that quantifies the heat distribution in the porous structure's solid matrix, which is separate from the fluid phase. Wu et al. [40] used the LTNE assumption to explore the impact of sinusoidal thermal boundary conditions with partial heating vertical walls on thermo-free convection in a porous domain occupied with a regular fluid. It was claimed that increasing the heat transfer coefficient between the two porous media phases, as well the heat conductivity ratio leads to the LTE situation in the porous medium. Chamkha et al. [11] investigated 2-D thermo-free-convection in a cavity with three parts: the first is solid, the second is filled with hybrid nanofluids, and the third is a porous layer loaded with hybrid nanofluid under LTNE condition. The natural convective heat transfer was observed to be increased as the portion of the cavity that is filled with the hybrid nanofluid expanded. Using the LTNE approach for the porous structure and Buongiorno's model for the nanofluid, Sheremet and Pop [36] investigated thermo-free convection in an angled porous chamber loaded with a nanofluid as a function of size and location of a hot part on the cavity bottom. It was discovered that reducing the gap between the hot part and the cold wall on the left could enhance the thermal exchange performance. Computational investigation via the Galerkin finite element method on thermo-buoyancy-driven convection within a porous cavity utilizing the LTNE and Darcy models is addressed by Mehryan et al. [27]. They found that decreasing nanoparticles' concentration and increasing modified thermal conductivity reduces the LTNE effects. Non-equilibrium thermal convective nanofluid transport features in a porous foam metal are simulated by Xu et al. [45]. Three different cases were considered. In another study, Xu et al. [44] conducted a CFD investigation of thermal convective transport along with an entropy generation analysis of a nanofluid in porous foams considering LTNE condition between the flowing nanofluid and the metal foam. Findings show that the Nusselt number rises with decreasing porosity and rising Reynolds number, permeability, the thermal conductivity of nanomaterials and solid matrix, and nanoparticles' concentration. Izadi et al. [24] used the LTNE model to simulate magneto-natural convective transport of a hybrid nanofluid flowing in a porous domain with two semi-cylindrical heat sources and two magnetic sources mounted to the walls. They suggested that the local thermal equilibrium model is justified at high Hartmann numbers. Alsabery et al. [7] elaborated a computational investigation of the thermo-buoyancy-driven convection in nanofluid-filled different porous domains with irregular walls by adopting the LTNE and the Forchheimer–Brinkman-extended Darcy designs. They evaluated the influence of involved physical parameters to demonstrate the LTNE effects within the porous domain. Ahmed [1] designed a CFD code based on Galerkin finite element method (FEM) to model the nanoliquid flow and thermal characteristics within an inclined anisotropic non-Darcy porous domain using the LTNE model. The thermal equilibrium state was confirmed to be validated for Nield numbers larger than 100. Izadi et al. [23] investigated thermal-free convection of CuO–water micropolar nanofluid inside a square domain filled with a porous media using the LTNE. They reached the conclusion that increasing the thermal conductivity ratio lowers the mixture's thermal resistance, which promotes the rate of heat exchange. The combination of the two heat transfer modes (convection and conduction) in a porous domain outside the local thermodynamic equilibrium saturated by a hybrid nanofluid was performed by Ghalambaz et al. [19]. They examined the effects of hybrid nanofluid and porous medium proprieties on the heat transfer inside the system. Ali et al. [5] employed the Galerkin finite element method to simulate thermo-free convection of nano-encapsulated phase change materials saturating porous media enclosed between two cylindrical cylinders under LTNE condition. Effects of Rayleigh number, Stefan number, melting point temperature, the concentration of

Table 1
Water-based fluid and copper nanomaterials properties [14,15].

	C_p(J/kg K)	λ (W/m K)	ρ(kg/m^3)	β (1/K)
Water (Pr = 6.2)	4179	0.613	997.1	21×10^{-5}
Cu (d_p = *30* nm)	385	401	8933	1.67×10^{-5}

the nanoparticles, cylinders' radii ratio, annulus's eccentricity, Darcy number, media's porosity, and non-dimensional heat transfer coefficient for the solid/nanofluid interface have been examined. A transient computational analysis of free convection in a partly porous chamber equipped with a thermo-generating/conducting portion on the bottom wall using the LTNE approach is carried out by Astanina et al. [8]. The influence of physical parameters on the heat transfer and the flow within the enclosure is investigated. Alomar et al. [6] studied laminar- thermo-buoyancy-driven convective flow in a non-Darcian porous square chamber equipped with L shape heated plate. It was found a strong influence of non-Darcian design and LTNE effects on the thermo-convection process within the domain. Recently, Wang et al. [39] constructed LB models for the thermo-buoyancy-driven convection process in a porous chamber with a circular cylinder using the LTNE approach. The temperature-dependent viscosity is investigated, and it was found to have a major impact on fluid and solid heat transfer. Other related works, such as in refs. [2,3,20,26,38] can be found in the literature.

Despite its significant engineering applications in the heat exchangers industry as well as in solar thermal installations, and previous research available to date, thermo-natural convection in porous annuli remains an issue that requires further investigation. Here, we were interested in assessing the effects of LTNE on thermo-free convection in a horizontal elliptical porous annulus saturated with a nanofluid. The outcomes have been evaluated for various porous medium properties under the LTNE condition. The standard 0.05 significance level was used to identify the LTE within the system. In addition, the spatial distribution contours of the LTNE sources within the porous annulus were represented.

2. Modeling approach

2.1. Physical model definition

The 2-D steady thermo-free convection problem in a porous annulus delimited by double horizontal elliptical cylinders with eccentricities of $e_1 = \frac{\sqrt{A_1^2 - B_1^2}}{A_1} = 0.9$ and $e_2 = \frac{\sqrt{A_2^2 - B_2^2}}{A_2} = 0.4$, respectively as sketched in Fig. 1. The internal surface having a constant hot temperature T_h, while the external surface is fixed at constant cold temperatures T_c. The domain's borders are considered to be impermeable. The Forchheimer–Brinkman-extended Darcy design, as well as the Boussinesq approximation, is considered. The convective heat transfer between the solid and the nanofluid phase is outside of LTNE situation. The heat transfer agent within the annulus is a water-based nanofluid containing copper nanomaterials. Table 1 gives the based liquid and nanomaterials properties [14,15].

2.2. Nanofluids properties

The following formulas are established to estimate the overall thermal properties of the employed nanoliquid:

$$\rho_{nf} = (1-\phi)\,\rho_f + \rho_{Cu}\phi \tag{1}$$

$$(\rho Cp)_{nf} = (1-\phi)\,(\rho Cp)_f + (\rho Cp)_{Cu}\phi \tag{2}$$

$$(\rho\beta)_{nf} = (1-\phi)\,(\rho\beta)_f + (\rho\beta)_{Cu}\phi \tag{3}$$

For the dynamic viscosity and heat conductivity, Corcione correlations were employed [12]:

$$\mu_{nf} = \mu_f/(1 - 34.87\left(d_{cu}/d_f\right)^{-0.3}(\phi_{Cu})^{1.03}) \tag{4}$$

Here: $d_f = 0.385$ nm is the diameter of water molecule

$$\lambda_{nf} = \lambda_f(1 + 4.4Re^{0.4}Pr^{0.66}\left(T/T_{fr}\right)^{10}\left(\lambda_{cu}/\lambda_f\right)^{0.03}(\phi_{Cu})^{0.66}) \tag{5}$$

Wherever, Re is determined as:

$$Re = 2k_b\rho_f T/\pi\mu_f^2 d_{cu} \tag{6}$$

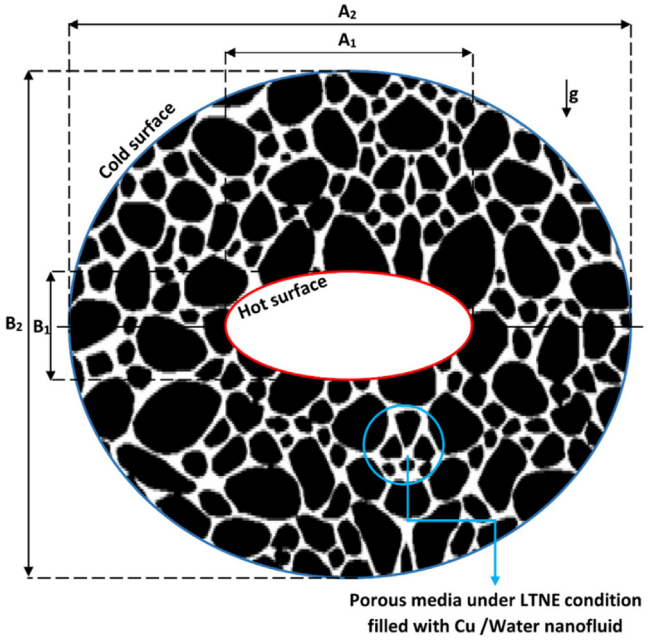

Fig. 1. Schematic diagram of the porous annulus system.

2.3. Governing equations

In the LTNE approach, heat transfer occurs between solid matrix and working nanofluid. In such an approach, two energy equations should be introduced. By considering the assumptions mentioned in the previous section, the motion and heat equations for the incompressible Newtonian nanofluid, steady state and laminar flow through a porous material can be formulated as:

$$\frac{\partial u}{\partial x}+\frac{\partial v}{\partial y}=0 \tag{7}$$

$$\frac{\rho_{nf}}{\varepsilon^2}\left(u\frac{\partial u}{\partial x}+v\frac{\partial u}{\partial y}\right)=-\frac{\partial p}{\partial x}+\frac{\mu_{nf}}{\varepsilon}\left(\frac{\partial^2 u}{\partial x^2}+\frac{\partial^2 u}{\partial y^2}\right)-\left(\frac{\mu_{nf}}{K}u-\frac{1.75}{\sqrt{150}\varepsilon^{3/2}}\frac{\rho_{nf}u\,|\mathbf{U}|}{\sqrt{K}}\right) \tag{8}$$

$$\frac{\rho_{nf}}{\varepsilon^2}(u\frac{\partial v}{\partial x}+v\frac{\partial v}{\partial y})=-\frac{\partial p}{\partial y}+\frac{\mu_{nf}}{\varepsilon}\left(\frac{\partial^2 v}{\partial x^2}+\frac{\partial^2 v}{\partial y^2}\right)-\left(\frac{\mu_{nf}}{K}v-\frac{1.75}{\sqrt{150}\varepsilon^{3/2}}\frac{\rho_{nf}v\,|\mathbf{U}|}{\sqrt{K}}\right)+(\rho\beta)_{nf}\,g(T_h-T_c) \tag{9}$$

$$u\frac{\partial T_f}{\partial x}+v\frac{\partial T_f}{\partial y}=\frac{\varepsilon\lambda_{nf}}{(\rho C_p)_{nf}}\left(\frac{\partial^2 T}{\partial x^2}+\frac{\partial^2 T}{\partial y^2}\right)+\frac{h(T_s-T_f)}{(\rho C_p)_{nf}} \tag{10}$$

$$(1-\varepsilon)\lambda_s\left(\frac{\partial^2 T_s}{\partial x^2}+\frac{\partial^2 T_s}{\partial y^2}\right)=h(T_s-T_f) \tag{11}$$

We define:

$$\begin{cases} u=\dfrac{\partial \psi}{\partial y} \\ v=-\dfrac{\partial \psi}{\partial x} \end{cases} \tag{12}$$

Here:

$$|\boldsymbol{U}|=\sqrt{u^2+v^2}$$

$$K=\frac{\varepsilon^3 d_m^3}{150(1-\varepsilon)^2}$$

d_m is the porous bed's mean particle size.

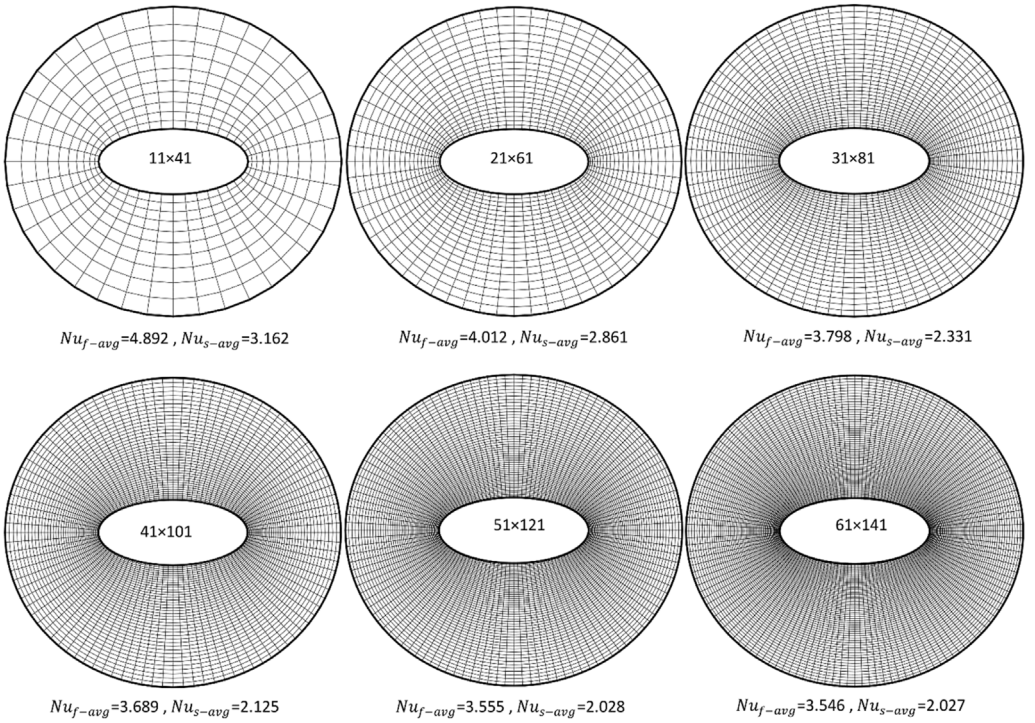

Fig. 2. Variation of the Nu_{f_avg} and Nu_{s_avg} with the grid size at Ra=10^5, Da=10^{-3} H = 1, $\gamma = 10$, $\phi = 0.02$, and ε=0.5.

We implemented the following dimensionless parameters to formulate the above equations in their non-dimensional form:

$$(X, Y) = \frac{(x, y)}{L}, \quad (U, V) = \frac{(u, v)}{\alpha_f} L, \quad P = \frac{p}{p_0}, \quad p_0 = \rho_f \frac{\alpha_f^2}{L^2}, \quad \theta = \frac{T_f - T_c}{T_h - T_c}, \quad \theta_s = \frac{T_s - T_c}{T_h - T_c},$$
$$\Psi = \frac{\psi}{\alpha_f}, \quad \lambda_{eff} = (1-\varepsilon)\lambda_s + \varepsilon\lambda_f, \quad \gamma = \frac{\varepsilon\lambda_f}{(1-\varepsilon)\lambda_s}, \quad H = \frac{hL}{\varepsilon k_f}, \quad F = \frac{1.75}{\varepsilon^{1.5}\sqrt{150}},$$
$$Ra = \frac{g\beta_f(T_h - T_c)L^3}{\upsilon_f \alpha_f}, \quad Pr = \frac{\upsilon_f}{\alpha_f}$$

With:

$$L = (A_2 - A_1)/2.$$

The dimensionless equations are written as follows:

$$\frac{\partial U}{\partial X} + \frac{\partial V}{\partial Y} = 0 \tag{13}$$

$$\frac{1}{\varepsilon^2}\left(U\frac{\partial U}{\partial X} + V\frac{\partial U}{\partial Y}\right) = -\frac{\partial P}{\partial X} + \frac{\rho_f}{\rho_{nf}}\frac{\mu_{nf}}{\mu_f}\frac{Pr}{\varepsilon}\left(\frac{\partial^2 U}{\partial X^2} + \frac{\partial^2 U}{\partial Y^2}\right) - \frac{\rho_f}{\rho_{nf}}\frac{\mu_{nf}}{\mu_f}\frac{Pr}{Da}U - \frac{F\sqrt{U^2+V^2}}{\sqrt{Da}}U \tag{14}$$

$$\frac{1}{\varepsilon^2}(U\frac{\partial V}{\partial X} + V\frac{\partial V}{\partial Y})$$

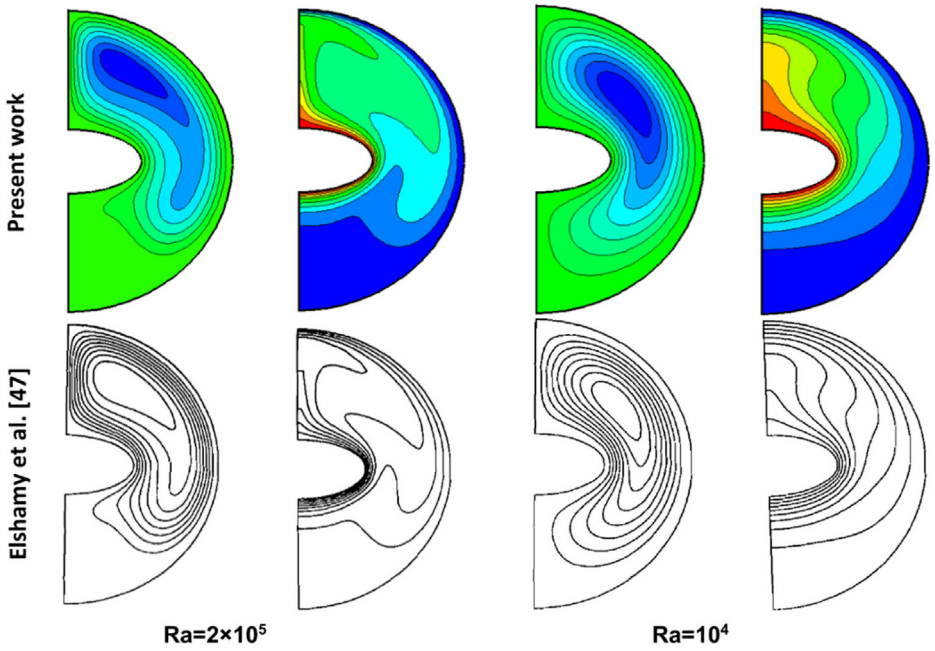

Fig. 3. Comparison of stream function and temperature isolines with Ref. [16] for two different Rayleigh.

$$= -\frac{\partial P}{\partial Y} + \frac{\rho_f}{\rho_{nf}}\frac{\mu_{nf}}{\mu_f}\frac{Pr}{\varepsilon}\left(\frac{\partial^2 V}{\partial X^2} + \frac{\partial^2 V}{\partial Y^2}\right) - \frac{\rho_f}{\rho_{nf}}\frac{\mu_{nf}}{\mu_f}\frac{Pr}{Da}U - \frac{F\sqrt{U^2+V^2}}{\sqrt{Da}}V$$
$$+ \frac{(\rho\beta)_{nf}}{\rho_{nf}\beta_f}Ra\,Pr\theta_f \tag{15}$$

$$\frac{1}{\varepsilon}\left(U\frac{\partial \theta_f}{\partial X} + V\frac{\partial \theta_f}{\partial Y}\right) = \frac{\lambda_{eff}}{\lambda_f}\frac{(\rho C_p)_f}{(\rho C_p)_{nf}}\left(\frac{\partial^2 \theta_f}{\partial X^2} + \frac{\partial^2 \theta_f}{\partial Y^2}\right) + \frac{(\rho C_p)_f}{(\rho C_p)_{nf}}H(\theta_s - \theta_f) \tag{16}$$

$$\frac{\partial^2 \theta_s}{\partial X^2} + \frac{\partial^2 \theta_s}{\partial Y^2} = +\gamma H(\theta_s - \theta_f) \tag{17}$$

$$\begin{cases} U = \dfrac{\partial \Psi}{\partial Y} \\ V = -\dfrac{\partial \Psi}{\partial X} \end{cases} \tag{18}$$

The dimensionless boundary conditions are written as:

$$\begin{cases} \text{Inner ellipse surface: } \mathrm{U} = \mathrm{V} = \Psi = 0 \quad \text{and} \quad \theta_s = \theta_f = 1 \\ \text{Outer ellipse surface: } \mathrm{U} = \mathrm{V} = \Psi = 0 \quad \text{and} \quad \theta_f = 0 \end{cases} \tag{19}$$

To evaluate the heat exchange rate, we calculate the local and mean Nusselt numbers on the hot ellipse as:

$$\begin{cases} Nu_f = \dfrac{\lambda_{eff}}{\lambda_f}\left(\dfrac{\partial \theta_f}{\partial n}\right)_n \\ Nu_s = \dfrac{\lambda_s}{\lambda_f}\left(\dfrac{\partial \theta_s}{\partial n}\right)_n \\ Nu_{f\_avg} = \dfrac{1}{s}\displaystyle\int_0^s Nu_f ds \\ Nu_{s\_avg} = \dfrac{1}{s}\displaystyle\int_0^s Nu_s ds \end{cases} \tag{20}$$

Where s is the dimensionless length along the hot ellipse surface.

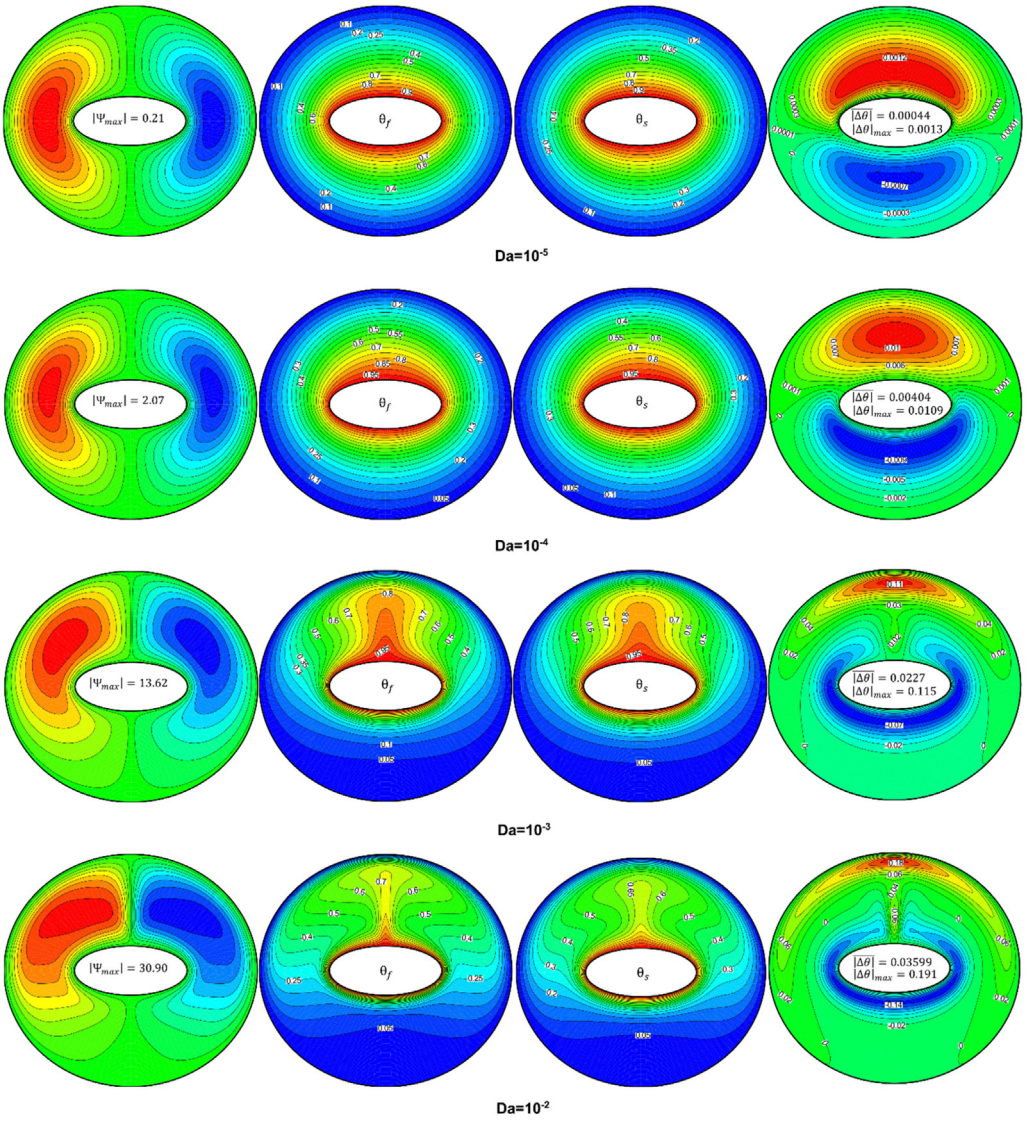

Fig. 4. Effect of Da on streamlines, fluid phase isothermal lines, solid phase isothermal lines, and non-equilibrium thermal source contours when Ra $= 10^5$, $\gamma = 10$, H $= 10$, and $\varepsilon = 0.5$.

3. Numerical approach and code validation

The non-dimensional transport equations that govern the solution of the problem are solved using the finite volume formulation [30]. The momentum and energy equations are solved by the second-order upwind method, whereas the pressure and velocity are coupled by SIMPLE algorithm. The under-relaxation technique is adopted to promote stability during the iteration process. A value of 10^{-6} was selected as a convergence criteria for all equations in order to obtain sufficiently accurate results. Grid sensitivity test was performed for the representative values of $Ra = 10^5$, $\varepsilon = 0.5$, $Da=10^{-3}$, $H=1$, $\gamma=10$ and $\phi=0.02$ to establish the independence of the grid on the numerical solutions. Results for mean Nusselt numbers of the two constituent phases of the porous structure considering various grid sizes are portrayed in Fig. 2. Consequently, a grid of 51 $\times$ 121 was retained. Further, our code was validated by comparing the computed numerical data quantitatively and qualitatively against results Elshamy et al. [16] (see Fig. 3 and Table 2).

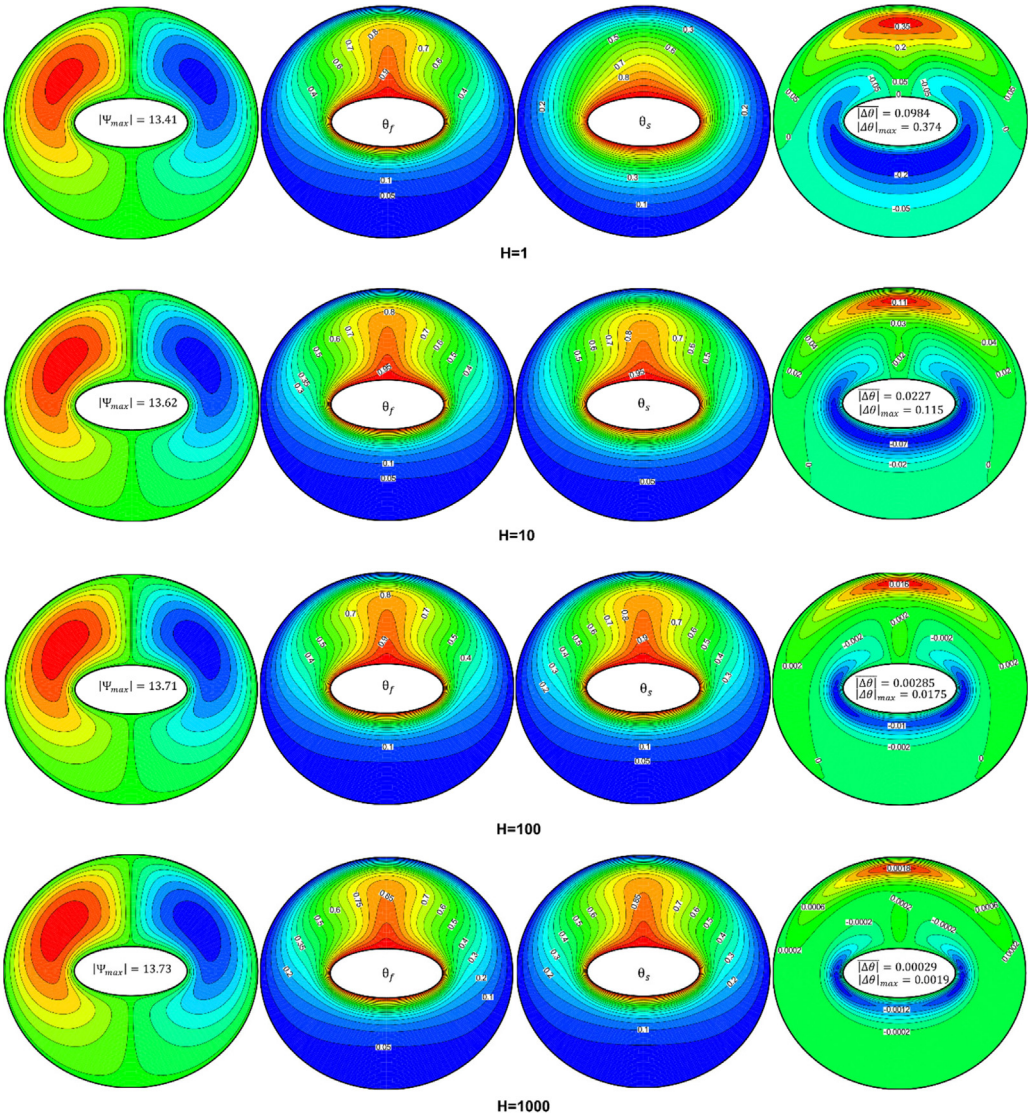

Fig. 5. Effect of H on streamlines, fluid phase isothermal lines, solid phase isothermal lines, and non-equilibrium thermal source contours when Ra $= 10^5$, Da=10^{-3}, $\gamma = 10$, and $\varepsilon = 0.5$.

Table 2
Comparison of mean Nusselt numbers with those observed by Ref. [16] for various values of Rayleigh.

	Our data			Ref. [16] ($Pr = 0.70$, $e_1 = 0.9$, $e_2 = 0.4$)		
Rayleigh (Ra)	10^4	6×10^4	2×10^5	10^4	6×10^4	2×10^5
Outer boundary	1.14	1.81	2.35	1.19	1.78	2.22
Inner boundary	3.53	5.48	7.21	3.53	5.5	7.25

4. Results and discussion

In the following section of the study, we attempt to examine the effects of LTNE condition between the phases of the porous structure on thermal-free convection inside a nanofluid-saturated elliptical porous annulus by reporting the effect of the relevant dimensionless parameters, e.g. Da, ε, H, and γ on streamlines, thermal distributions in the fluid of the fluid and solid mediums, non-equilibrium thermal source contours, flow intensity, and heat transfer rates

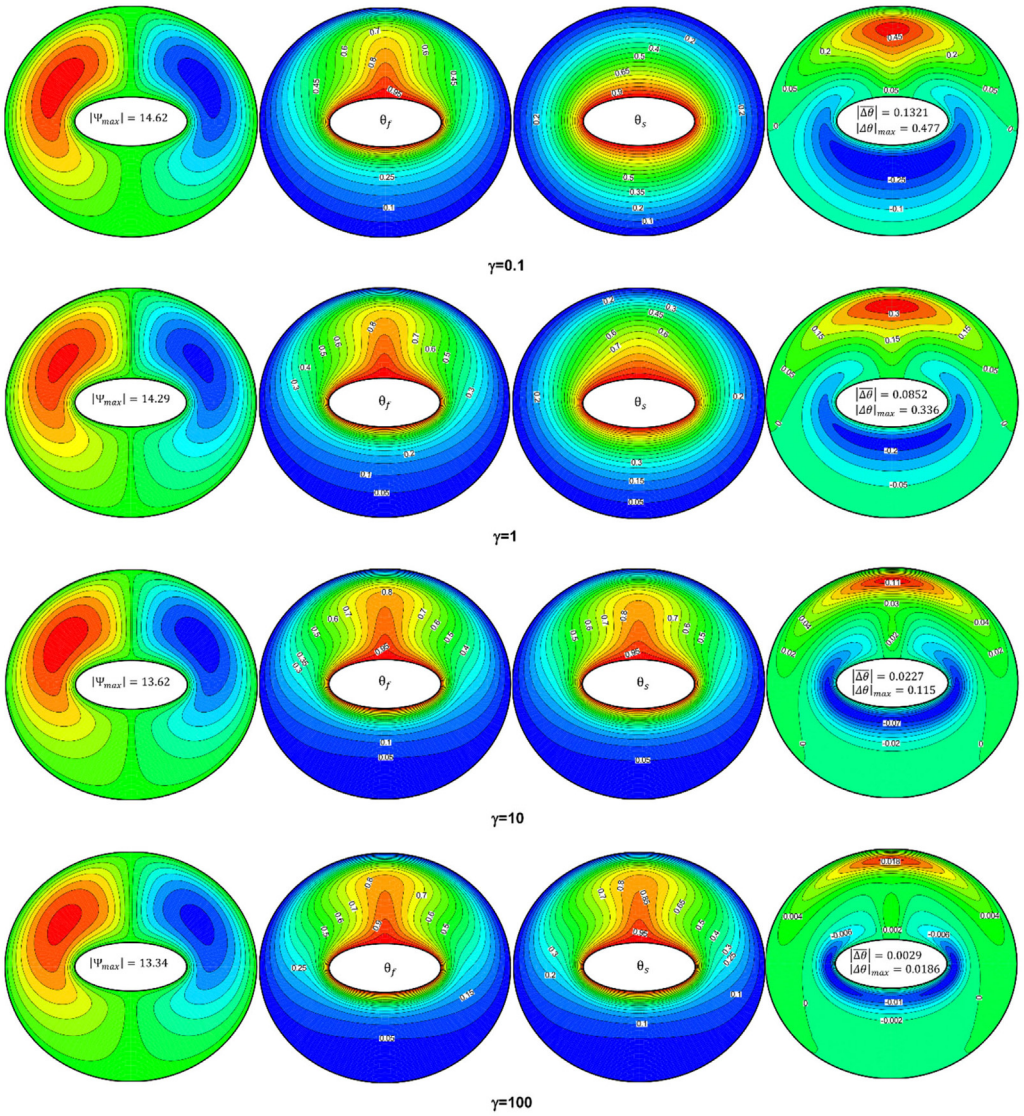

Fig. 6. Effect of γ on streamlines, fluid phase isothermal lines, solid phase isothermal lines, and non-equilibrium thermal source contours when Ra $= 10^5$, Da=10^{-3}, H $= 10$, and $\varepsilon = 0.5$.

at a given Rayleigh number (Ra=10^5) and nanomaterials concentration in the water ($\phi = 0.02$). The isothermal maps of the nanofluid phase are the results of Eq. (16), which describe the solution of the dimensionless heat equation within the nanofluid phase, and the isothermal maps of the solid matrix are the results of Eq. (17) which describe the solution of the dimensionless heat equation in the solid phase of the porous structure. Also, in order to accurately identify the spatial distribution of the LTNE sources within the porous medium, several criteria have been admitted in the literature. The criterion adopted in this study is based on the difference in local temperatures of the fluid phase and the solid phase at each point in the computational domain. The dimensionless temperature differences maps $\Delta\theta = (\theta_f - \theta_s)$ through which we can delineate the zones where there is a LTE and the zones where there is a LTNE are graphically plotted. Besides, the absolute temperature differences are averaged on the total volume of the domain as: $\left|\overline{\Delta\theta}\right| = \frac{1}{V}\int \left|(\theta_f - \theta_s)\right| dV$. Based on the standard 0.05 significance level, a result value lower than 0.05 means that the LTE case is verified.

Fig. 4 depicts the effects of the Darcy parameter (Da) on the stream function isolines (Ψ), isothermal lines of the fluid phase (θ_f), isothermal lines of the solid phase (θ_s), and non-equilibrium thermal source contours within

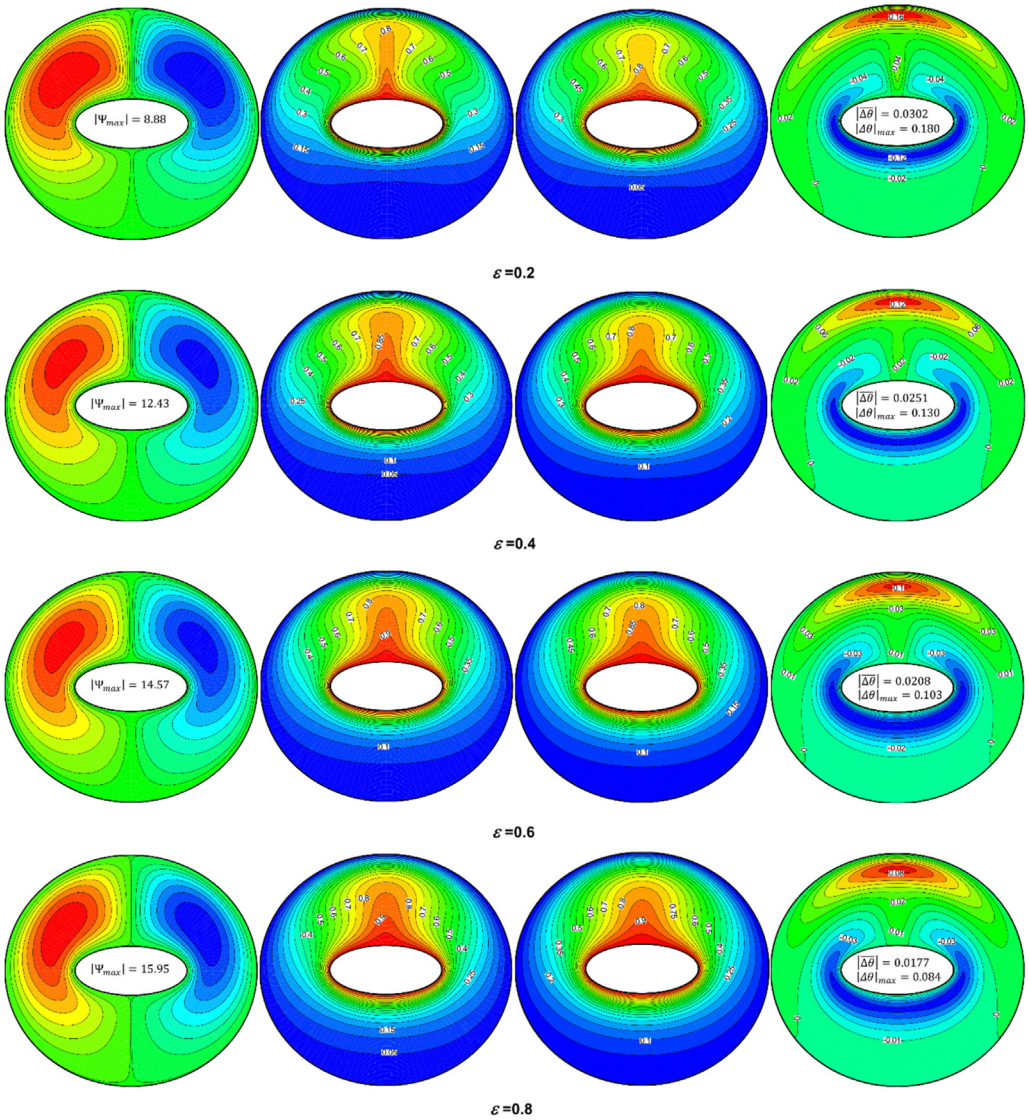

Fig. 7. Effect of ε on streamlines, fluid phase isothermal lines, solid phase isothermal lines, and non-equilibrium thermal source contours when Ra $= 10^5$, Da=10^{-3}, $\gamma = 10$, and H $= 10$.

the porous medium ($\Delta\theta$) at a given non-dimensional heat transfer coefficient for the solid/nanofluid interface (H $= 10$), modified thermal conductivity ($\gamma = 10$), and porosity ($\varepsilon = 0.5$). The streamlines show that the flow forms a symmetric pair of counter-rotating vortices within the porous annulus under the effect of the buoyancy-driven motion generated between the hot internal boundary and the cold external boundary for all Darcy numbers. It is also seen that for the low magnitude of Darcy number, due to low permeability, the streamlines demonstrated a very weak nanofluid circulation because the porous matrix restricts the flow and prevents the nanofluid from freely permeating through the porous medium, resulting in weak flow circulation. Besides that, the isotherms of both phases in the annulus are almost parallel, concentric, and correspond to the active walls, indicating that the heat transfer occurs essentially by the conduction mode. In this stage, heat is observed to be simply distributed from the hot inner boundary to the cold outer boundary through the porous annulus. When Darcy's number increases, the porous matrix provides less resistance to the nanofluid motion, the convection enhances, and the mode of heat transfer shifts from conductive mode at low Da into convective mode at high Da. It should be noted that an inactive flow region (inert zone) has formed at the lower extremity of the porous annulus.

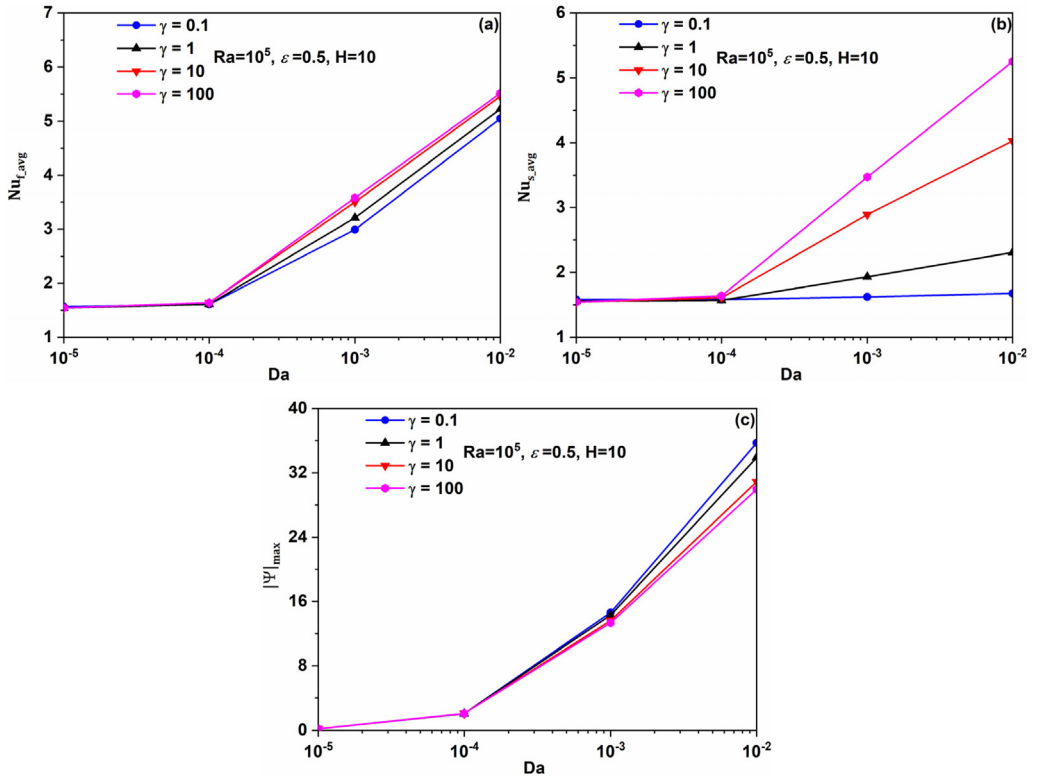

Fig. 8. Effect of Da on Nu_{f_avg}, Nu_{s_avg}, and $|\Psi_{max}|$ when Ra $= 10^5$, H $= 10$, $\varepsilon = 0.5$.

Moreover, at low Da, the dimensionless fluid-to-solid temperature differences contours, ($\Delta\theta$) in Fig. 4 show that the highest LTNE source zones are visible in the lower portion of the porous annulus (with negative values indicating that the solid temperatures are greater than those of the nanofluid) and in the upper part of the annulus (with positive values indicating that the nanofluid temperatures are greater than those of the solid), while the lowest LTNE source zones are on both sides of the annulus. As the Darcy number increases, the highest LTNE source zone in the upper region rises toward the top of the annulus and expands along the cold outer surface, while the highest LTNE source zone in the bottom region stretches along the hot inner surface except for the thermal plume that develops on the top of the hot ellipse. At this stage, LTE can be found in the inactive region in the lower extremity of the porous annulus. The values of $\left|\overline{\Delta\theta}\right|$ and $\left|\overline{\Delta\theta}\right|_{max}$ are found to be augmented with Da indicating that the effects of the LTNE are more important at high Darcy numbers, resulting in a notable difference in the isothermal lines' distribution between the two phases in the porous annulus. Furthermore, regarding the values of $\left|\overline{\Delta\theta}\right|$, and since are less than the standard 0.05 significance level, it can be stated that the LTE case is considered verified in the entire porous system for all values of Da when H $= 10$, $\gamma = 10$, and $\varepsilon = 0.5$.

The implications of the non-dimensional heat transfer coefficient for the solid/nanofluid interface (H) on the streamlines, isothermal lines distribution of nanofluid and solid phases, and dimensionless temperature differences contours inside the porous annulus are depicted in Fig. 5. The other parameters are kept constant as Da=10^{-3}, $\gamma = 10$, and $\varepsilon = 0.5$. As shown, increasing H raises the stream function's maximum value, implying that the convection is enhanced due to improved thermo-exchange nanofluid/solid matrix within the porous annulus. Furthermore, augmenting H causes the temperature difference between the nanofluid phase and the solid phase in the porous annulus to be as small as possible, implying that increasing H makes the LTE situation easier to achieve, or in another word, the LTE approach would be adequate at higher values of H. Besides that, as shown by the $\left|\overline{\Delta\theta}\right|$ values in this figure, LTE is considered verified in the entire porous annulus for H > 10.

Fig. 6 shows the consequences of the change in the thermal conductivity ratio (γ) on Ψ, θ_f, θ_s, and ($\Delta\theta$). An examination of this figure reveals that the nanofluid flow circulation decreases with γ. This is because augmenting

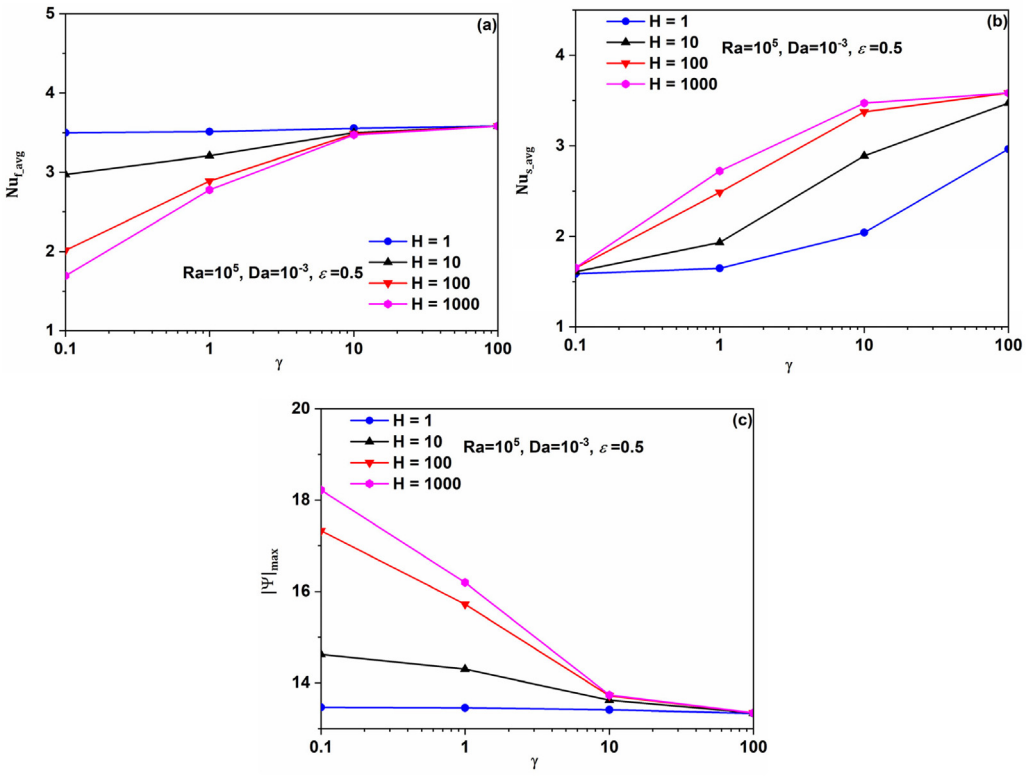

Fig. 9. Effect of H and γ on Nu_{f_avg}, Nu_{s_avg}, and $|\Psi_{max}|$ when Ra $= 10^5$, Da=10^{-3}, $\varepsilon = 0.5$.

the heat conductivity of the nanofluid phase increases the amount of heat transfer compensation between phases. As a result, more thermal energy is lost which leads to a weaker convective flow. Consequently, when the ratio of thermal conductivity between the two phases is very low, the convective heat transfer between the solid matrix and the nanofluid is weak, and hence, the LTNE effects are found to be at their strongest and attained at large distances. It is also possible to indicate that the situation of the LTE in the entire system is verified for γ >10 though H is weak (H = 10) as one can see it by the values of $|\overline{\Delta\theta}|$.

According to Fig. 7, the flow motion within the porous annulus is observed to be augmented as the media's porosity value increases, since a porous medium with a high porosity provides more ability for the fluid to move freely within the annulus. Changing ε parameter has little effect on the shape of the flow vortices relative to their strength. In addition, LTNE effects become even larger when ε takes smaller values.

Fig. 8 describes the mean Nusselt numbers for the fluid phase (Nu_{f_avg}) and the solid phase (Nu_{s_avg}), and flow strength flow intensity ($|\Psi_{max}|$) variations with Da for different γ when Ra $= 10^5$, H = 10, $\varepsilon = 0.5$. It is clear that as Da augments, for a given γ, the mean Nusselt number of both nanofluid and solid phases augments, notably for Da $> 10^{-4}$ because of a stronger nanofluid circulation. The converging values of Nu_{f_avg} and Nu_{s_avg} at lower Da signal the LTE situation, as previously stated. The effects of γ on Nusselt numbers are more significant for high Da values with more important progression for Nu_{s_avg}. It can also be seen that the nanofluid circulation strength increases with Da at a given γ and decreases with γ at given Da.

Effects of H and γ on Nu_{f_avg}, Nu_{s_avg}, and $|\Psi_{max}|$ when Ra $= 10^5$, Da=10^{-3}, $\varepsilon = 0.5$ are portrayed in Fig. 9. Through these curves, we realize that at low values of γ especially, Nu_{f_avg} undergoes a rapid decrease with H, while Nu_{s_avg} follows an inverse behavior due to the fact that the decrease in Nu_{f_avg} is compensated by an increase in Nu_{s_avg}. It is to note that at high values of γ, Nu_{f_avg} becomes independent of H, while Nu_{s_avg} increase with H for all values of γ except for $\gamma = 0.1$. Besides, Nu_{f_avg} is observed to increase with γ for all values of H, except for lower H (H = 1) where Nu_{f_avg} is found independent of γ, while Nu_{s_avg} increase with γ for all H values. Further, the nanofluid circulation decreases rapidly with γ, notably for high H values where the heat transfer compensation

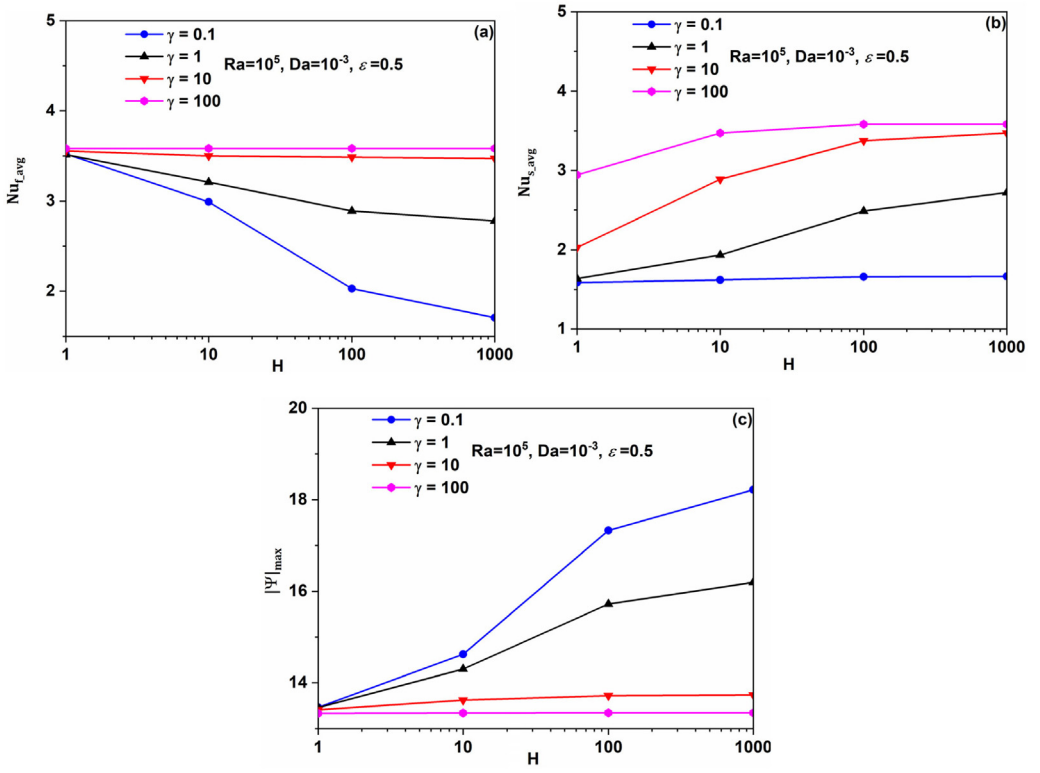

Fig. 9. (*continued*).

between phases of the porous medium is at its maximum. While, the intensity of the nanofluid recirculation within the annulus enhances as H increase and becomes independent of H for high values of γ.

Fig. 10(a)–(b) show that the decrease in the porosity (ε) causes an increase in the average Nusselt numbers (Nu_{f_avg} and Nu_{s_avg}). This can be attributed to the enhancement in the porous medium's effective heat conductivity. Moreover, as is seen in Fig. 10(c), the natural convective nanofluid flow is improved with the increment in the ε parameter

Table 3 presents some benchmark results for the case of (Ra $= 10^5$ and $\varepsilon = 0.5$). The results confirm that the higher the value of Da and the smaller value of H and γ, the higher are the LTNE effects.

5. Conclusion

The following outstanding results were obtained through this investigation:

- Increasing Da, and ϵ lead to an enhancement of the thermo-natural convective circulation of nanofluid within the porous annulus irrespective of the values of γ and H.
- The nanofluid circulation is found to increase with H until it becomes independent of it for high values of γ, and it decreases with γ, notably for large values of H.
- Heat transfer rate can be enhanced for both phases within the porous annulus by increasing Da, notably for Da $> 10^{-4}$.
- Nu_{f_avg} can be decreased by increasing H. The decrease in Nu_{f_avg} is compensated by an increase in Nu_{s_avg}. When the parameter γ is high enough, Nu_{f_avg} is independent of the H parameter.
- Increasing γ is accompanied by a rise in Nu_{s_avg}. Additionally, increasing γ improves Nu_{f_avg}, which is particularly noticeable when H is high.
- Increasing ε is accompanied by a diminish in both Nu_{s_avg} and Nu_{f_avg}.

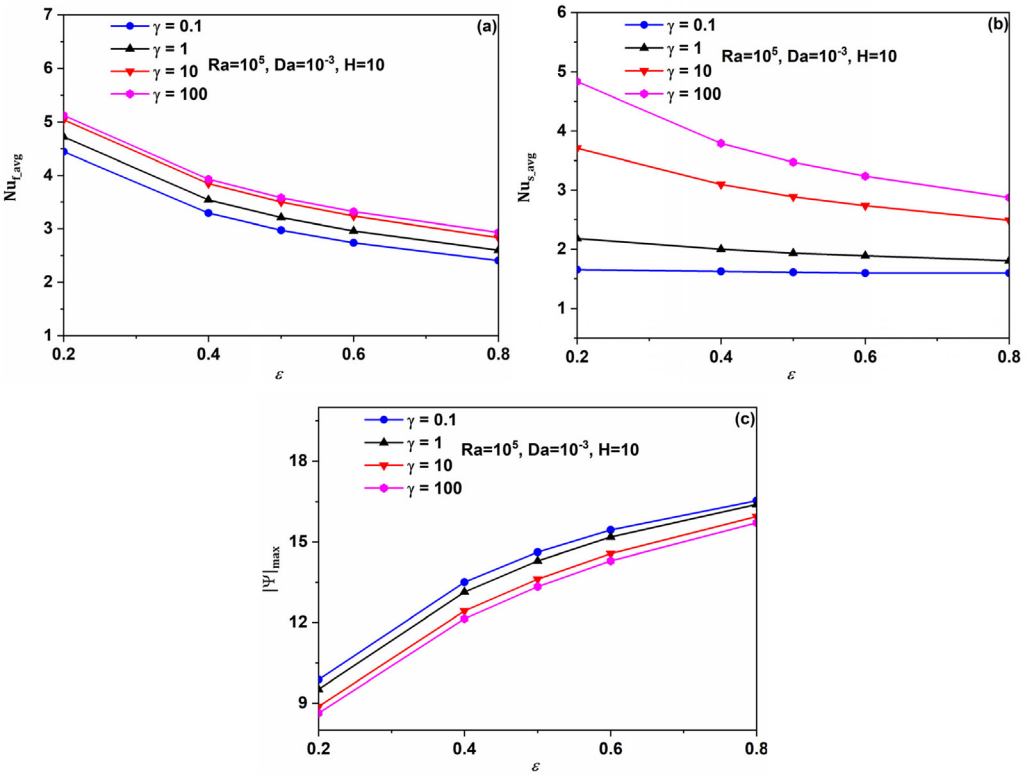

Fig. 10. Effect of ε on Nu_{f_avg}, Nu_{s_avg}, and $|\Psi_{max}|$ when Ra $= 10^5$, Da $=10^{-3}$, H $= 10$.

- High LNTE effects sources are located at the top of the porous annulus with $\theta_f > \theta_s$, and at the bottom with $\theta_s > \theta_f$. The values of $\left|\overline{\Delta\theta}\right|$ and $\left|\overline{\Delta\theta}\right|_{max}$ are found to be augmented by augmenting Da and diminishing H, γ and ε.
- LTNE effects were suggested to be more significant at higher Da
- The higher the value of Da and the smaller value of H, γ and ε, the higher are the LTNE effects.

Nomenclature

• A	Ellipse's major axis (m)
• B	Ellipse's minor axis (m)
• C_p	Massic heat capacity (J/kg K)
• Da	Darcy number
• F	Forchheimer coefficient
• H	Heat transfer coefficient for the solid/nanofluid interface
• g	Gravitational acceleration (m/s^{-2})
• K	Permeability (m^2)
• k_b	Boltzmann's constant, 1.380648×10^{-23} (J/K)
• L	Characteristic length (m)
• p, P	Pressure (Pascal) and dimensionless pressure
• T	Temperature (K)
• T_{fr}	Freezing point of the base liquid (K)
• u, v	Velocities (m/s)
• U, V	Nondimensional velocities

Table 3
Benchmark results for $\overline{|(\Delta\theta)|}$ when Ra = 10^5 and $\varepsilon = 0.5$.

	Da	γ	H=1	H=10	H=100	H=1000
Ra=10^5	10^{-5}	0.1	0.00604	0.00293	0.00048	0.00005
		1	0.00545	0.00193	0.00026	0.000028
		10	0.00276	0.00044	0.000048	0.000005
		100	0.00047	0.000052	0.0000055	0.0000007
	10^{-4}	0.1	0.05519	0.02701	0.00447	0.00048
		1	0.04976	0.0177	0.002422	0.00025
		10	0.02519	0.00404	0.000436	0.00004
		100	0.00433	0.00047	0.0000476	0.000004
	10^{-3}	0.1	0.1898	0.1321	0.03507	0.00414
		1	0.1732	0.0852	0.01735	0.00203
		10	0.0984	0.0227	0.00285	0.00029
		100	0.0235	0.00297	0.00030	0.00003
	10^{-2}	0.1	0.21376	0.17507	0.08905	0.01818
		1	0.19907	0.12062	0.03279	0.00429
		10	0.12796	0.03599	0.00497	0.00052
		100	0.03638	0.00507	0.00053	0.00005
LTNE case						LTE case

- x, y Cartesian coordinate system (m)
- X, Y Nondimensional Cartesian coordinate system

Greek letters

- α Thermal diffusivity (m^2/s)
- β Thermal expansion coefficient (1/K)
- γ Modified thermal conductivity ratio
- ϕ Solid fraction of the nanomaterials
- θ Nondimensional temperature
- ψ, Ψ Stream function (m^2/s) and dimensionless stream function

- λ Thermal conductivity (W/m K)
- μ Fluid dynamic viscosity (kg/m s)
- υ Fluid kinematic viscosity (Pa s)
- ρ Density (kg/m^3)
- ε Porosity of the porous medium

Subscripts

- *avg* Average
- *c* Cold
- *Cu* Copper
- *f* Fluid (water)
- *h* Hot
- *p* Porous
- *nf* Nanoliquid
- *s* Solid

Abbreviations

- LTE Local Thermal Equilibrium
- LTNE Local Thermal Non-Equilibrium

References

[1] S.E. Ahmed, FEM-CBS algorithm for convective transport of nanofluids in inclined enclosures filled with anisotropic non-Darcy porous media using LTNEM, Internat. J. Numer. Methods Heat Fluid Flow 31 (1) (2020) 570–594.

[2] S.E. Ahmed, Non-darcian natural convection of a nanofluid due to triangular fins within trapezoidal enclosures partially filled with a thermal non-equilibrium porous layer, J. Therm. Anal. Calorim. 145 (5) (2021) 2691–2706.

[3] S.E. Ahmed, M.M. Abd El-Aziz, Effect of local thermal non-equilibrium on unsteady heat transfer by natural convection of a nanofluid over a vertical wavy surface, Meccanica 48 (1) (2013) 33–43.

[4] S.E. Ahmed, M.A. Mansour, A.M. Rashad, T. Salah, MHD natural convection from two heating modes in fined triangular enclosures filled with porous media using nanofluids, J. Therm. Anal. Calorim. 139 (5) (2020) 3133–3149.

[5] F.H. Ali, H.K. Hamzah, M. Mozaffari, S.A.M. Mehryan, M. Ghalambaz, Natural convection of nanoencapsulated phase change suspensions inside a local thermal non-equilibrium porous annulus, J. Therm. Anal. Calorim. 141 (5) (2020) 1801–1816.

[6] O.R. Alomar, N.M. Basher, A.A. Yousif, Analysis of effects of thermal non-equilibrium and non-Darcy flow on natural convection in a square porous enclosure provided with a heated l shape plate, Int. J. Mech. Sci. 181 (2020) 105704.

[7] A.I. Alsabery, T. Tayebi, A.J. Chamkha, I. Hashim, Natural convection of Al_2O_3-water nanofluid in a non-Darcian wavy porous cavity under the local thermal non-equilibrium condition, Sci. Rep. 10 (1) (2020) 1–22.

[8] M.S. Astanina, M. Sheremet, C.J. Umavathi, Unsteady natural convection in a partially porous cavity having a heat-generating source using local thermal non-equilibrium model, Internat. J. Numer. Methods Heat Fluid Flow 29 (6) (2019) 1902–1919.

[9] I.A. Badruddin, A.A. Al-Rashed, N.S. Ahmed, S. Kamangar, K. Jeevan, Natural convection in a square porous annulus, Int. J. Heat Mass Transfer 55 (23–24) (2012) 7175–7187.

[10] V.V. Calmidi, R.L. Mahajan, Forced convection in high porosity metal foams, J. Heat Transf. 122 (3) (2000) 557–565.

[11] A.J. Chamkha, S. Sazegar, E. Jamesahar, M. Ghalambaz, Thermal non-equilibrium heat transfer modeling of hybrid nanofluids in a structure composed of the layers of solid and porous media and free nanofluids, Energies 12 (3) (2019) 541.

[12] M. Corcione, Empirical correlating equations for predicting the effective thermal conductivity and dynamic viscosity of nanofluids, Energy Convers. Manage. 52 (1) (2011) 789–793.

[13] D.D. Dinčov, K.A. Parrott, K.A. Pericleous, Heat and mass transfer in two-phase porous materials under intensive microwave heating, J. Food Eng. 65 (3) (2004) 403–412.

[14] A.S. Dogonchi, A.J. Chamkha, D.D. Ganji, A numerical investigation of magneto-hydrodynamic natural convection of Cu–water nanofluid in a wavy cavity using CVFEM, J. Therm. Anal. Calorim. 135 (4) (2019) 2599–2611.

[15] A.S. Dogonchi, M.A. Ismael, A.J. Chamkha, D.D. Ganji, Numerical analysis of natural convection of Cu–water nanofluid filling triangular cavity with semicircular bottom wall, J. Therm. Anal. Calorim. 135 (6) (2019) 3485–3497.

[16] M.M. Elshamy, M.N. Ozisik, J.P. Coulter, Correlation for laminar natural convection between confocal horizontal elliptical cylinders, Numer. Heat Transfer 18 (1) (1990) 95–112, http://dx.doi.org/10.1080/10407789008944785.

[17] M.H. Esfe, M. Bahiraei, H. Hajbarati, M. Valadkhani, A comprehensive review on convective heat transfer of nanofluids in porous media: Energy-related and thermohydraulic characteristics, Appl. Therm. Eng. 178 (2020) 115487.

[18] X.B. Feng, Q. Liu, Y.L. He, Numerical simulations of convection heat transfer in porous media using a cascaded lattice Boltzmann method, Int. J. Heat Mass Transfer 151 (2020) 119410.

[19] M. Ghalambaz, M.A. Sheremet, S.A.M. Mehryan, F.M. Kashkooli, I. Pop, Local thermal non-equilibrium analysis of conjugate free convection within a porous enclosure occupied with Ag–MgO hybrid nanofluid, J. Therm. Anal. Calorim. 135 (2) (2019) 1381–1398.

[20] N.S. Gibanov, M.A. Sheremet, H.F. Oztop, N. Abu-Hamdeh, Effect of uniform inclined magnetic field on mixed convection in a lid-driven cavity having a horizontal porous layer saturated with a ferrofluid, Int. J. Heat Mass Transfer 114 (2017) 1086–1097.

[21] M. Izadi, B. Bastani, M.A. Sheremet, Numerical simulation of thermogravitational energy transport of a hybrid nanoliquid within a porous triangular chamber using the two-phase mixture approach, Adv. Powder Technol. 31 (6) (2020) 2493–2504.
[22] M. Izadi, M. Javanahram, S.M.H. Zadeh, D. Jing, Hydrodynamic and heat transfer properties of magnetic fluid in porous medium considering nanoparticle shapes and magnetic field-dependent viscosity, Chin. J. Chem. Eng. 28 (2) (2020) 329–339.
[23] M. Izadi, S.A.M. Mehryan, M.A. Sheremet, Natural convection of CuO-water micropolar nanofluids inside a porous enclosure using local thermal non-equilibrium condition, J. Taiwan Inst. Chem. Eng. 88 (2018) 89–103.
[24] M. Izadi, R. Mohebbi, H. Sajjadi, A.A. Delouei, LTNE modeling of magneto-ferro natural convection inside a porous enclosure exposed to nonuniform magnetic field, Physica A 535 (2019) 122394.
[25] R.A. Mahdi, H.A. Mohammed, K.M. Munisamy, N.H. Saeid, Review of convection heat transfer and fluid flow in porous media with nanofluid, Renew. Sustain. Energy Rev. 41 (2015) 715–734.
[26] M.A. Mansour, M.M. Abd El-Aziz, R.A. Mohamed, S.E. Ahmed, Numerical simulation of natural convection in wavy porous cavities under the influence of thermal radiation using a thermal non-equilibrium model, Transp. Porous Media 86 (2) (2011) 585–600.
[27] S.A.M. Mehryan, M. Ghalambaz, A.J. Chamkha, M. Izadi, Numerical study on natural convection of Ag–MgO hybrid/water nanofluid inside a porous enclosure: A local thermal non-equilibrium model, Powder Technol. 367 (2020) 443–455.
[28] Y. Menni, A.J. Chamkha, A. Azzi, Nanofluid transport in porous media: a review, Special Top. Rev. Porous Media: Int. J. 10 (1) (2019).
[29] R. Mohebbi, A.A. Delouei, A. Jamali, M. Izadi, A.A. Mohamad, Pore-scale simulation of non-Newtonian power-law fluid flow and forced convection in partially porous media: thermal lattice Boltzmann method, Physica A 525 (2019) 642–656.
[30] S.V. Patankar, Numerical Heat Transfer and Fluid Flow, McGraw-Hill, New York, 1980.
[31] G.K. Ramesh, S.A. Shehzad, M. Izadi, Thermal transport of hybrid liquid over thin needle with heat sink/source and Darcy–Forchheimer porous medium aspects, Arab. J. Sci. Eng. 45 (11) (2020) 9569–9578.
[32] Z.Z. Rashed, S.E. Ahmed, Z.A.S. Raizah, Thermal dispersion and buongiorno's nanofluid model effects on natural convection in an inclined rectangular enclosure partially filled with heat generating porous medium, J. Porous Media 23 (4) (2020).
[33] S. Rashidi, J.A. Esfahani, N. Karimi, Porous materials in building energy technologies—A review of the applications, modelling and experiments, Renew. Sustain. Energy Rev. 91 (2018) 229–247.
[34] S. Rashidi, J.A. Esfahani, A. Rashidi, A review on the applications of porous materials in solar energy systems, Renew. Sustain. Energy Rev. 73 (2017) 1198–1210.
[35] H. Sajjadi, A.A. Delouei, R. Mohebbi, M. Izadi, S. Succi, Natural convection heat transfer in a porous cavity with sinusoidal temperature distribution using Cu/water nanofluid: Double MRT lattice Boltzmann method, Commun. Comput. Phys. 29 (1) (2021) 292–318.
[36] M.A. Sheremet, I. Pop, Effect of local heater size and position on natural convection in a tilted nanofluid porous cavity using LTNE and Buongiorno's models, J. Molecular Liquids 266 (2018) 19–28.
[37] R.L. Van Dam, C.T. Simmons, D.W. Hyndman, W.W. Wood, Natural free convection in porous media: First field documentation in groundwater, Geophys. Res. Lett. 36 (11) (2009).
[38] Y. Varol, H.F. Oztop, M. Mobedi, I. Pop, Visualization of natural convection heat transport using heatline method in porous non-isothermally heated triangular cavity, Int. J. Heat Mass Transfer 51 (21–22) (2008) 5040–5051.
[39] L. Wang, C. Huang, J. Hu, B. Shi, Z. Chai, Effects of temperature-dependent viscosity on natural convection in a porous cavity with a circular cylinder under local thermal non-equilibrium condition, Int. J. Therm. Sci. 159 (2021) 106570.
[40] F. Wu, G. Wang, W. Zhou, Buoyancy induced convection in a porous cavity with sinusoidally and partially thermally active sidewalls under local thermal non-equilibrium condition, Int. Commun. Heat Mass Transfer 75 (2016) 100–114.
[41] Z.B. Xing, X. Han, H. Ke, Q.G. Zhang, Z. Zhang, H. Xu, F. Wang, Multi-phase lattice Boltzmann (LB) simulation for convective transport of nanofluids in porous structures with phase interactions, Internat. J. Numer. Methods Heat Fluid Flow 31 (8) (2021) 2754–2788.
[42] Q. Xiong, T. Tayebi, M. Izadi, A.A. Siddiqui, T. Ambreen, L.K. Li, Numerical analysis of porous flat plate solar collector under thermal radiation and hybrid nanoparticles using two-phase model, Sustain. Energy Technol. Assess. 47 (2021) 101404.
[43] H. Xu, Z. Xing, The lattice Boltzmann modeling on the nanofluid natural convective transport in a cavity filled with a porous foam, Int. Commun. Heat Mass Transfer 89 (2017) 73–82.
[44] H. Xu, Z.B. Xing, A. Ghahremannezhad, Lattice Boltzmann modeling on forced convective heat transfer of nanofluids in highly conductive foam metals with local thermal nonequilibrium (LTNE) effect, J. Porous Media 22 (12) (2019) 1553–1571.
[45] H. Xu, Z. Xing, K. Vafai, Analytical considerations of flow/thermal coupling of nanofluids in foam metals with local thermal non-equilibrium (LTNE) phenomena and inhomogeneous nanoparticle distribution, Int. J. Heat Fluid Flow 77 (2019) 242–255.
[46] S.R. Yan, M. Izadi, M.A. Sheremet, I. Pop, H.F. Oztop, M. Afrand, Inclined Lorentz force impact on convective-radiative heat exchange of micropolar nanofluid inside a porous enclosure with tilted elliptical heater, Int. Commun. Heat Mass Transfer 117 (2020) 104762.
[47] S.E. Zorrilla, A.C. Rubiolo, Mathematical modeling for immersion chilling and freezing of foods: Part I: model development, J. Food Eng. 66 (3) (2005) 329–338.